LA-UR-17-27333

Title: Cavitation Bubble Interacting with a Richtmyer-Meshkov Unstable Sheet and Spike

Author(s): Buttler, William Tillman; Renner, Dru Bryant; Morris, Christopher; Manzanares, Ruben; Anderson, Eric Karl; Goett, John Jerome III; Heidemann, Joel A.; Kalas, Ryan Matthew; Llobet Megias, Anna; Martinez, John Israel; Medina, Patrick Vernon Jr.; Payton, Jeremy Ronald; Saunders, Alexander; Schmidt, Derek William; Tainter, Amy Marie; Tupa, Dale; Vincent, Samuel Walker; McNeil, Wendy Vogan

Intended for: 20th Biennial APS Conference on Shock Compression of Condensed Matter, 2017-07-10/2017-07-14 (St. Louis, Missouri, United States)

Issued: 2018-07-30 (rev.1)

Cavitation Bubble Interacting with a Richtmyer-Meshkov Unstable Sheet and Spike

W. T. Buttler[1,a)], D. Renner[1], C. Morris[1], R. Manzanares[1], E. K. Anderson[1], J. J. Goett III[1], J. Heidemann[1], R. M. Kalas[1], A. Llobet[1], J. I. Martinez[1], P. V. Medina Jr.[1], J. R. Payton[1], A. Saunders[1], D. W. Schmidt[1], A. M. Tainter[1], D. Tupa[1], S. W. Vincent[1] and W. Vogan-McNeil[1]

[1]*Los Alamos National Laboratory, PO Box 1663, Los Alamos, New Mexico 87545, USA*

a)buttler@lanl.gov

Abstract. We study dynamic interactions between a shock-induced Sn cavitation bubble with a Richtmyer-Meshkov unstable (RMU) sheet and spike in explosively driven, colliding shockwave, cylindrical geometries. The Sn surface finishes were mirror like and smooth, or included a scallop- or divot-perturbation in the Sn above the collision axis. In all cases a cavitation bubble formed in the Sn, with an RMU-sheet or -spike on the scallop- and divot-tests: the unstable sheet sliced the bubble open, but the spike punctured it. As the shockwaves released from the perturbation a cavitation-wave transverse to the shockwave formed, sourcing mass into the sheet and spike. In the case of the divot test, the transverse cavitation wave penetrated through the Al cylinder, releasing Al and HE products beyond the cylinder surface. Surprisingly, on the divot test the cavitation bubble imploded, sealing the ruptured tube after a few microseconds.

INTRODUCTION

Three high explosive (HE) driven, colliding-wave FICH (feature instability cavitation history) experiments were fielded in cylindrical geometries at the LANSCE proton radiography (pRad) facility [1]. The geometry included two coincidentally detonated RP-1 detonators in contact with PBX 9501, which was surrounded by concentric metal tubes. The inner tube was Al, while the outer was Ta and included Sn on the mid-plane test section. On one test, the "null" test, the Sn finish was smooth and unperturbed, but the other tests included a divot above, or scallop about, the mid-plane. All tests formed an unstable cavitation bubble in the Sn (see Fig. 1), while the scallop- and divot-tests formed a Richtmyer-Meshkov [2, 3] unstable (RMU) sheet or spike inside the bubble.

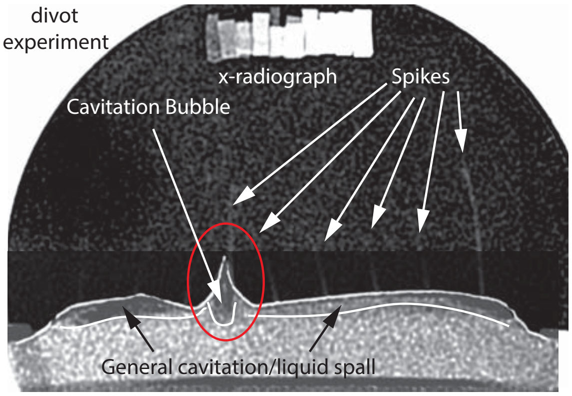

FIGURE 1. X-ray radiograph of flat-plate colliding shockwave and divot dynamics (PBX 9501, Al-6061, Sn).

Shock Compression of Condensed Matter - 2017
AIP Conf. Proc. 1979, 080003-1–080003-6; https://doi.org/10.1063/1.5044845
Published by AIP Publishing. 978-0-7354-1693-2/$30.00

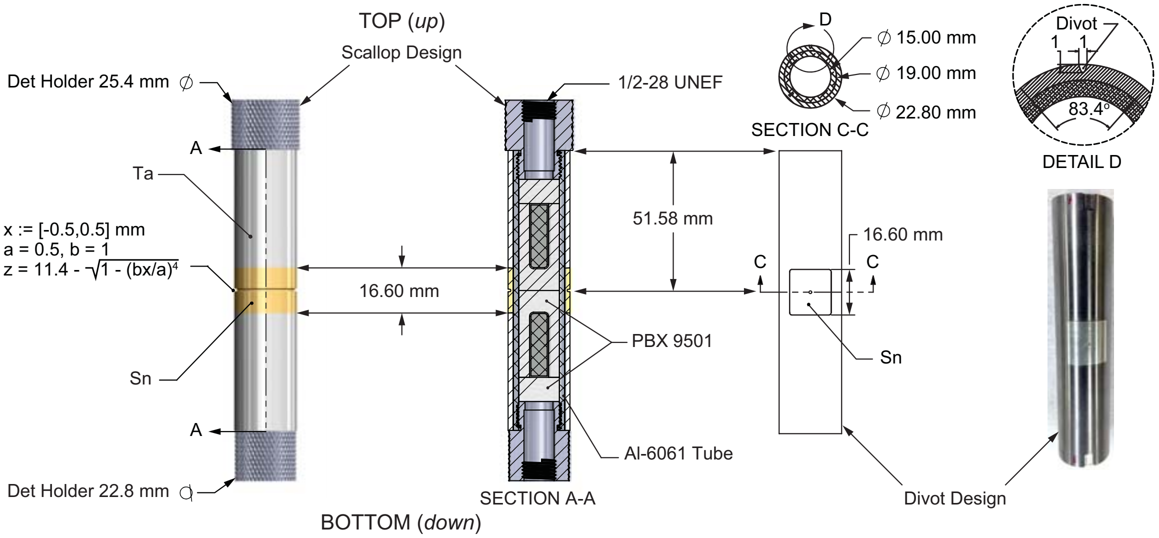

FIGURE 2. The FICH design (see the text for details); *up* and *down* indicates the orientation in the pRad vessel.

The experiments were designed to evaluate whether dynamics incidental to RM instabilities would breach the HE products cavity confined within the Al, Ta and Sn cylindrical assemblies, and release HE products from the perturbation locations. Importantly, our initial simulations predicted the cavitation bubble seen on all three tests, but not the sub-surface dynamics on the scallop- and divot-tests, nor the rupture and release of HE products beyond the tubing surface on the divot test.

EXPERIMENTAL DETAILS

The basic geometry of the null, scallop and divot-tests (pRad0655, pRad0656 and pRad0631, respectively) has been discussed. Not mentioned earlier is that two Ta slugs were embedded in the HE to support loading pressures on the bomb's mid-plane, and that the geometry of the divot-test assembly was different than the null- and scallop-tests, as seen in Fig. 2.

The FICH Design

Figure 2 shows the scallop- and divot-assembly diagrams. The Ta slugs embedded in the HE are seen in SECTION A-A in Fig. 2, and detailed in Fig. 3. Two RP-1 detonators (not shown) were positioned in contact with the 8.9 mm tall PBX 9501 boosters, one at the *up*- and one at the *down*-end. Gaps between the Al, HE and Ta slugs were filled with Sylgard 184 (from Dow Corning). Excepting the scallop, the null- and scallop-geometries were identical.

Diagnostics

The diagnostics included laser Doppler velocimetry (LDV) [4–9] and proton radiography [1]. Each experiment acquired 31 proton radiographs and included 21 LDV probes normally aligned to the cylinder's surface in seven circumferential rows of three probes, with a central row on the mid-plane axis, and three rows above (*up*) and below (*down*). From the axis the three *up*- and three *down*-rows were at ±4, ±14 and ±20 mm, arranged in three columns of seven probes rotated ±120° from each other. Considering Fig. 2, +120° was clockwise, and −120° was counter-clockwise from above. The LDV data are used to validate hydrodynamic simulations.

Proton Radiograph Timing.

The proton radiograph timing sought to capture the detonation waves prior to arriving at the bomb mid-plane, with nominal interframe times between radiographs of $\sim 0.250\ \mu$s, but the interframe times on the last 8 frames were varied to 0.35 μs on the null test, and 0.5 μs on the divot-test, with the total imaging time after shockwave breakout on the mid-plane axis being $\sim 7.25\ \mu$s on all tests.

LDV Common Timing.

The LDV data were commonly timed to a current viewing resistor (CVR). This meant that the signals, which were recorded on multiple scopes, had a unique correction factor to accurately time the signals and radiographs. Time comparisons of the data are inconsistent but the surface velocimetry are quantitative.

Pre-Shot Predictions

Based on the bomb geometry, for the Ta we expected shock loading pressures of $P_S^{\mathrm{Ta}}(\pm 20\ \mathrm{mm}) \approx P_S^{\mathrm{Ta}}(\pm 14\ \mathrm{mm}) \approx 16$ GPa, and for the Sn we expected $P_S^{\mathrm{Sn}}(\pm 4\ \mathrm{mm}) \approx 12$ GPa, and $P_S^{\mathrm{Sn}}(0\ \mathrm{mm}) \approx 24$ GPa on the mid-plane; in all cases the Ta is solid on shock and release, but the Sn is solid on shock and release ±4 mm off the mid-plane and solid on shock and releasing to a mixed solid-liquid phase on the mid-plane axis. These P_S^{Ta} and P_S^{Sn} give $u^{\mathrm{Ta}}(\pm 20\ \mathrm{mm}) = u^{\mathrm{Ta}}(\pm 14\ \mathrm{mm}) \approx 0.5$, $u^{\mathrm{Sn}}(\pm 4\ \mathrm{mm}) \approx 1.0$ and $u_{fs} \equiv u^{\mathrm{Sn}}(0\ \mathrm{mm}) \approx 1.75\ \mathrm{mm}/\mu\mathrm{s}$. The 2D and 3D physics in [10, 11] with u_{fs} predict $u^p_{sht} = U^p_{sht} + u_{fs} \approx 3.9$ and $u^p_{spk} = U^p_{spk} + u_{fs} = \sqrt{3}U^p_{sht} + u_{fs} \approx 5.5\ \mathrm{mm}/\mu\mathrm{s}$, where U^p_{sht} and U^p_{spk} are rest frame sheet (2D) and spike (3D) velocities.

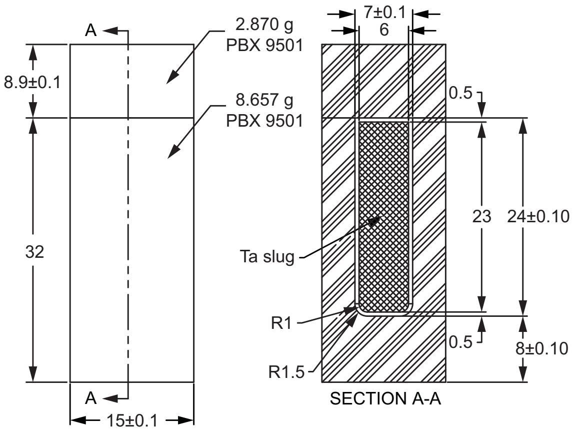

FIGURE 3. HE and Ta slug assembly.

RESULTS

The detonators and HE were carefully positioned, and alignment of the LDV probes was within ±100 μm of design locations, which means the time of shockwave breakout at the Ta and Sn surfaces should be accurate to within ±15 ns. The first surface motion in the velocimetry is inconsistent, but the radiographs demonstrate that the shockwaves arrived on axis within ±10 ns on the three tests implying ±25 ns in velocimetry.

Velocimetry

The 0° column data for all tests are seen in Fig. 4. The solid black traces are on the package mid-plane, and the half-tone, blue, and red traces are ±4 (Sn), ±14 (Ta) and ±20 mm (Ta) off the mid-plane, respectively; dashed lines are oriented "up" and solid lines "down." All data are quantitative. The pRad0655 (null) data infer incoincident initiation of the detonators, but analysis of the radiographs demonstrates excellent end-to-end timing, within ±10 ns on the mid-plane on all experiments.

The pRad0655 (null) and pRad0656 (scallop) data show that the cavitation bubble and RMU sheet reached their measured asymptotic velocities of $u^m_{cb} = U^m_{cb} + u_{fs} = 2.25$ and $u^m_{sht} = U^m_{sht} + u_{fs} = 4.1$ mm/μs after about 0.2- and 1-μs, respectively, implying $U^m_{cb} \approx 0.5$ mm/μs and $U^m_{sht} \approx 2.35 > U^p_{sht} = 2.15$ mm/μs predicted in [10].

On pRad0631 (divot) the spike velocity should be $U^m_{spk} = \sqrt{3}U^m_{sht}$ [11], therefore, we expect $u^m_{spk} \approx \sqrt{3}U^m_{sht} + u_{fs} = 5.8$ mm/μs, similar to observation but $u^m_{spk} > u^p_{spk} = 5.5$ mm/μs; u^m_{spk} achieved its asymptotic after about 1.5 μs.

Proton Radiography

Figure 5 shows three radiographs each from pRad0655, pRad0656 and pRad0631. The Al and Sn cylinder boundaries (interfaces) are identified in the radiographs.

The pRad0655 (null) radiographs show that a cavitation bubble similar to that seen in Fig. 1 encompasses the mid-plane axis.

The pRad0656 (scallop) radiographs show the shockwaves in the HE and metals (red dashed lines) under the scallop ($t = 0$ μs). By 2 μs the RMU mass source is seen as a transverse-cavitation-wave (TCW) that has stagnated on the Al surface, and the RMU sheet has split the cavitation bubble open. By 4 μs a bifurcation in the RMU sheet, which may have been caused as the sheet split the cavitation bubble open, is seen.

The pRad0631 (divot) dynamics reveal a cavitation bubble, an RMU spike and a TCW that sources mass into the RMU spike. The radiographs show that within 2 μs the TCW perforated the Sn and Al cylinders into the HE products cavity. Also by this time, the RMU spike – which is too thin and fast to be seen in the radiographs – has punctured the cavitation bubble. By 4 μs the cavitation bubble has almost completely collapsed—imploded, and dense material is seen jetting beyond the bubble. By 7.25 μs the bubble implosion is complete, the breach has sealed, but dense material is still seen beyond the surface.

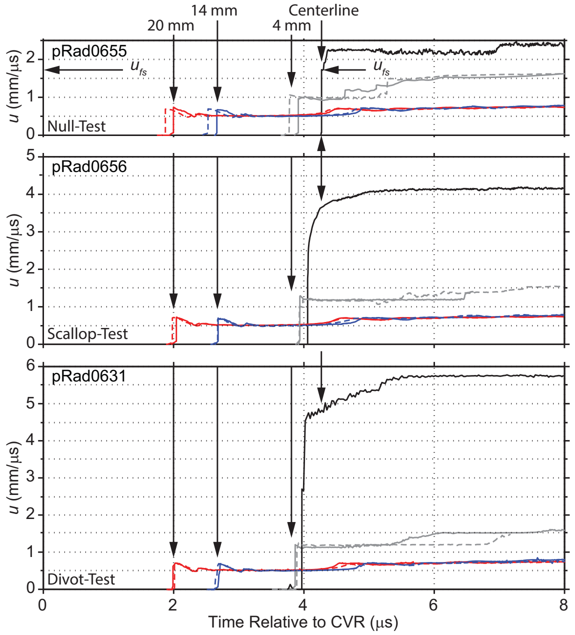

FIGURE 4. The 0° column LDV FICH data.

CONCLUSIONS

The FICH experiments returned excellent, quantitative velocimetry, but questions about common timing remain, especially on pRad0655.

The proton radiographs reveal the formation of a cavitation bubble on all tests. The scallop- and divot-tests show that an RMU sheet or spike forms inside of the cavitation bubble, and that the instability quickly splits the bubble open (sheet) or punctures it (spike). The scallop- and divot-test radiographs also reveal that a cavitation wave forms transverse to the shockwaves in the material. The TCW develops as the shockwaves

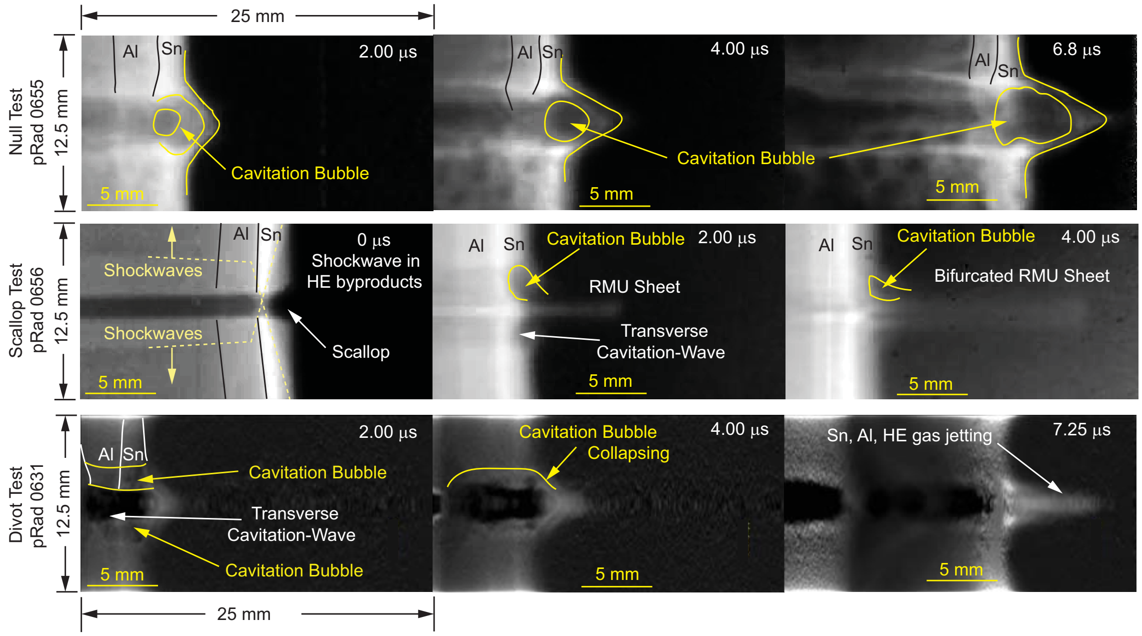

FIGURE 5. The time on the upper right of each proton radiograph is the time at which the radiograph was acquired relative to when the shockwaves arrived beneath the Sn surface. The Sn, Al boundaries, transverse cavitation wave, cavitation bubble, RMU sheet and HE gases jetting beyond the divot-test surface are identified.

interact with the scallop and divot (shock and release), sourcing mass into the RM sheet and spike as they grow beyond the exploding cylinder surface; the TCW velocity is bounded by the material sound speeds. In the case of the scallop, the TCW stagnates on the Al, but on the divot test the TCW penetrates through the Al into the HE products cavity, releasing what appears to be HE gases and Al beyond the cylinder surface. Finally, the most interesting phenomena observed is on the divot-test, where the RMU spike is seen to pierce the cavitation bubble, causing it to implode at late times: cavitation bubble collapse.

ACKNOWLEDGMENTS

Many thanks to the pRad core team for their efforts and support to make these experiments a success.

By acceptance of this article, the publisher recognizes that the U.S. Government retains a nonexclusive, royalty free license to publish or reproduce the published form of this contribution, or to allow others to do so, for U.S. Government purposes. Los Alamos National Laboratory requests that the publisher identify this article as work performed under the auspices of the U.S. Department of Energy Los Alamos National Laboratory, an affirmative action/equal opportunity employer, is operated by Los Alamos National Security, LLC, for the National Nuclear Security Administration of the U.S. Department of Energy under contract DE-AC52-06NA25396.

REFERENCES

[1] A. Gavron, C. L. Morris, and H. J. Zumbro, “Proton radiography,” Tech. Rep. LA-UR-96-420 (Los Alamos National Laboratory, 1996).

[2] R. D. Richtmyer, Comm. Pure Appl. Math. **XIII**, 297–319 (1960).

[3] E. E. Meshkov, Akad. Nauk SSSR, Mekh. Zhidk. Gasa **5**, 151–158 (1969).

[4] H. Cummins, N. Knable, L. Gampel, and Y. Yeh, Appl. Phys. Lett. **2**, 62–64 (1963).

[5] H. Cummins, N. Knable, and Y. Yeh, Appl. Opt. **2**, 823–825 (1963).

[6] Y. Yeh and H. Z. Cummins, Appl. Phys. Lett. **4**, 176–178 (1964).

[7] J. W. F. Jr., E. W. George, and R. D. Lewis, Appl. Phys. Lett. **7**, 77–78 (1965).

[8] W. T. Buttler, S. K. Lamoreaux, F. G. Omenetto, and J. R. Torgerson, “Optical velocimetry,” Tech. Rep. LA-UR-04-6453 (Los Alamos National Laboratory, 2004).

[9] T. O. Strand, D. R. Goosman, C. Martinez, and T. L. Whitworth, Rev. Sci. Instrum. **77**, p. 083108 (2006).

[10] W. T. Buttler, D. M. Oró, D. L. Preston, K. O. Mikaelian, F. J. Cherne, R. S. Hixson, F. G. Mariam, C. Morris, J. B. Stone, G. Terrones, and D. Tupa, J. Fluid Mech. **703**, 60–84 (2012).

[11] K. O. Mikaelian, Phys. Rev. Lett. **80**, 508–511 (1998).